Characterization, modelling and mitigation of gene expression burden in mammalian cells

Frei T[1]±, Cella F[2,3]±, Tedeschi F[2], Gutierrez J[1], Stan GB[4], Khammash M[1]*, Siciliano V[2]*.

1 Department of Biosystems Science and Engineering, ETH Zürich
2 Istituto Italiano di Tecnologia-IIT, Largo Barsanti e Matteucci, Naples ITA
3 University of Genoa, Genoa ITA
4 Department of Bioengineering and Centre for Synthetic Biology, Imperial College London, U.K.
± These authors contributed equally
*Co-corresponding authors: mustafa.khammash@bsse.ethz.ch and velia.siciliano@iit.it

Abstract

Despite recent advances in genome engineering, the design of genetic circuits in mammalian cells is still painstakingly slow and fraught with inexplicable failures. Here we demonstrate that competition for limited transcriptional and translational resources dynamically couples otherwise independent co-expressed exogenous genes, leading to diminished performance and contributing to the divergence between intended and actual function. We also show that the expression of endogenous genes is likewise impacted when genetic payloads are expressed in the host cells. Guided by a resource-aware mathematical model and our experimental finding that post-transcriptional regulators have a large capacity for resource redistribution, we identify and engineer natural and synthetic miRNA-based incoherent feedforward loop (iFFL) circuits that mitigate gene expression burden. The implementation of these circuits features the novel use of endogenous miRNAs as integral components of the engineered iFFL device, a versatile hybrid design that allows burden mitigation to be achieved across different cell-lines with minimal resource requirements. This study establishes the foundations for context-aware prediction and improvement of *in vivo* synthetic circuit performance, paving the way towards more rational synthetic construct design in mammalian cells.

Introduction

Mammalian synthetic biology facilitates the study of diverse biological processes including gene regulation[1], developmental patterns[2], and cancer progression[3]. More recently, it has gained clinical relevance, offering powerful new tools for the engineering of recombinant protein-producing cells[4] and for the creation of novel cell-based therapies for clinical use[5–7]. These critical applications require synthetic gene circuits that are robust and predictable with minimal impact on their host cells. However, engineering such circuits requires numerous design-build-test-learn iterations[8,9], which are particularly expensive and time consuming[10] in mammalian cells.

At the core of the problem is the poor predictability of gene expression[9] in engineered cells arising from the dependence of gene expression on the cellular context. In particular, the often overlooked dependence of exogenous genetic circuits on limited host resources that are shared with endogenous pathways frequently leads to unanticipated and counterintuitive circuit behaviors[11]. In bacterial cells, substantial progress towards increasing the predictability of gene expression has been made by showing that exogenous genetic material imposes a significant burden, resulting in decreased growth rates and degraded cellular performance[12]. This has been attributed to the diversion of the pool of resources available for gene expression[13,14] towards transcription and translation of the newly introduced synthetic payloads. These observations prompted the development of models that consider gene expression in a resource-limited context[15–18] and led to approaches for mitigating the impact of resource burden in bacteria[19,20]. Analogous studies in *S. Cerevisiae* showed that transcription and translation are limiting processes[21]. In mammalian cells, while performance shortcomings of synthetic circuits due to transactivator dosage and plasmid uptake variation[22] have been observed, a deeper understanding of the problem of resource burden and methods for its mitigation are still missing. Moreover, competition for endogenous resources might have detrimental effects on basic and translational biology. For instance, in studies based on transient DNA expression, genes that are used to normalize the results might be subject to resource-dependent expression coupling (e.g protein levels measured by flow cytometry are usually normalized to the expression levels of the transfection marker, which is also used as a measure of transfection efficiency).

Here, we investigate the burden imposed by synthetic circuits on host cells (**Fig. 1**). Through the design of genetic constructs that allow us to uncouple transcription and translation processes, we separately study transcriptional and translational burden caused by cellular resource sharing. In particular, we engineer several regulatory circuits composed of a tunable load, called *X-tra* (eXtra Transgene), which we genetically express in the host cell in varying amounts. We then measure the impact of this tunable load on a 'sensor' gene, which we refer to as the *capacity monitor* (**Fig. 1a**). We demonstrate in different mammalian cell lines that the sharing of transcriptional and

translational resources in the host cell can tightly couple otherwise independently co-expressed synthetic genes and lead to trade-offs in their expression (**Fig. 1a**)**.** To enhance the predictability of synthetic devices in mammalian cells, we explicitly incorporate these load sharing effects in a general mathematical model in which we replace the rates of resource-dependent reactions with adjusted *effective* rates (**Fig. 1b**). We demonstrate that such a resource-aware model successfully recapitulates the observed, and sometimes unexpected, dose-responses of the various genetic circuits we tested. Additionally, we investigate the role of post-transcriptional regulators, like RNA-binding proteins (RBPs) and microRNAs (miRNAs) in mitigating the impact of burden-induced coupling and find that both are able to reallocate resources, making them candidates for use in burden-mitigation circuits. Using these observations, and guided by our modelling framework, we identify the *incoherent Feed-Forward Loop* (iFFL) as a network topology that is particularly effective at resource burden mitigation, and then we use endogenous and synthetic microRNA (miRNA) regulation to engineer iFFL-based, burden-mitigating synthetic circuits (**Fig. 1c**). While miRNA-based iFFL circuits have been previously constructed to buffer gene expression against noise[23] and fluctuations in external inducer concentration[24,25], in this study we demonstrate for the first time that they also act to rescue the expression level of genes of interest despite changes in available cellular resources due to the loading effects of transgene constructs (**Fig. 1c**).

To the best of our knowledge this is the first study to characterize the individual transcriptional and translational burden contributions induced by exogenous gene expression in mammalian cells, and to unveil mechanisms of resource reallocation for burden mitigation using post-transcriptional regulation. The study also pioneers the use of *endogenous* miRNAs as integral parts of synthetic circuits, which in our case consist of iFFL burden-mitigation devices. Together with a refined mathematical modelling framework that describes biochemical reactions in the context of finite resources, these findings pave the way to more realistic output predictions and optimal synthetic construct design in mammalian cells.

Results

Genetic circuits impose a burden on mammalian cells as they compete for limited shared cellular resources

We reasoned that due to competition for finite cellular resources, there is a threshold above which gene expression from synthetic circuits saturates. To test this, we co-transfected HEK293T cells with two constitutively expressed fluorescent proteins mCitrine and mRuby3 driven by EF1α promoters, in molar ratios ranging from 1:4 to 4:1, for a total of 50 ng (low) or 500 ng (high) of encoding plasmid (**Fig. 2a**). Model-based computer simulations of the expected response in the presence of

competition for limited resources are presented (**Fig. 2a, left**). The equations used to generate these plots were derived from the modelling framework introduced later on in **Fig. 4a** (**Supplementary Note 1**). In accordance with the simulations, the total amount of 500 ng of encoding plasmids results in a dramatic drop in experimentally measured global gene expression as compared to 50 ng (**Fig. 2a, right**). Furthermore, in both experimental conditions mCitrine and mRuby3 fluorescence levels are negatively correlated; the higher the amount of expressed mCitrine, the lower that of mRuby3 and vice versa (**Fig. 2a, right**); this correlation was also more severe for 500 ng of transfected plasmid than for 50 ng.

We demonstrated that the negative correlation is cell-type and promoter independent by expressing in H1299, U2OS, HeLa, HEK293T and CHO-K1 cell lines, *X-tra* and *capacity monitor* both driven by the constitutive promoter CMV, in molar ratios ranging from 1:1 to 2.5:1, for a total of 500 ng of encoding plasmids (**Supplementary Fig. 1-4, 14a**). Further, by using a PGK promoter[26] that has different expression strength compared to CMV in HEK293T and H1299 (**Supplementary Fig. 5a**), we observed analogous outcomes (**Supplementary Fig. 5b,c**). Finally, by combining different molar ratios of mCitrine and mRuby3 encoding plasmids driven by two promoters of different strengths (EF1α or EFS) a similar behavior to **Fig. 2a** was observed (**Supplementary Fig. 6**).

As many synthetic circuits rely on tunable gene expression, we next tested resource competition on transcriptional inducible systems, by modulating *X-tra* repression with a Doxycycline (Dox)-repressed promoter (**Fig. 2b**) at different concentrations of Dox (from 0 to 1 μg/mL) while keeping *capacity monitor* amounts constant (**Fig. 2b, left**). Consistent with previous results, we observed that increased repression of *X-tra* corresponds to increased *capacity monitor* levels (**Fig. 2b, right**).

To exclude any experimental confounds as the source of our observations, we demonstrated that neither cell seeding nor nutrient supply had any apparent effect on the expression levels of the two genes, one of which was titrated whereas the second was held at a constant copy number (**Supplementary Fig. 7**).

These proof-of-concept experiments demonstrate that: *i)* gene expression in mammalian synthetic circuits is connected even in the absence of direct regulation, and *ii)* expression of exogenous genes is limited by cellular resource availability.

Both transcriptional and translational resources are limiting

Since several different resource pools could be responsible for the observed effects described above, we set out to characterize the individual contributions of transcriptional and translational resource limitation to cellular burden. To evaluate potential limitations in transcriptional resources and the consequent gene competition for mRNA expression, we quantified mRNA levels in cells expressing *X-tra*/*capacity monitor* molar ratios from 1:1 to 2.5:1 in H1299 cells for a total of 500ng of plasmid

127 DNA (corresponding protein data in **Supplementary Fig. 1**). We observed that as the *X-tra* mRNA
128 increased, the *capacity monitor* mRNA levels decreased (**Fig. 2c**), supporting the hypothesis that
129 shared transcriptional resources are indeed a limiting factor in mammalian synthetic gene
130 co-expression.

131 To investigate whether the expression of endogenous genes is also affected by heterologous
132 genetic payloads, we transfected H1299 cells with a plasmid encoding for EGFP and mKate under the
133 control of a bidirectional promoter. We then sorted transfected cells according to *high* and
134 *intermediate* levels of fluorescent markers, as well as *non-transfected* cells (absence of fluorescence)
135 (**Supplementary Fig. 8**). We then quantified the mRNA levels of 3 endogenous genes (CyCA2, eIF4E,
136 GAPDH, **Fig. 2d**). Notably, in transfected cells that express *high* and *intermediate* levels of EGFP and
137 mKate, the expression of CyCA2, eIF4E and GAPDH decreases when compared to the *non-transfected*
138 population. We also measured the mRNA levels of CyCA2, eIF4E and GAPDH in cells transfected with
139 *X-tra*/*capacity monitor* molar ratios from 1:1 to 2:1 and observed a progressive, albeit not dramatic
140 decrease with higher amounts of *X-tra* when compared to the 1:1 ratio (**Supplementary Fig. 9**). In
141 this case cells were not sorted before mRNA extraction.

142 To provide further support to the observations on transcriptional burden on exogenous
143 genes (**Fig. 2c**), we implemented a genetic circuit that can selectively overload the transcriptional
144 resource pool without sequestering translational resources. The system is based on the self-cleaving
145 hepatitis delta virus (HDV) ribozyme, which ensures that most of the transcribed mRNA is cleaved
146 and thus destabilized (**Fig. 2e, left**). The circuit is composed of a single plasmid with two
147 transcriptional units (TUs). One TU contains a tTA transcription factor co-expressed with the mRuby3
148 (*capacity monitor*) via the P2A peptide, driven by a constitutive promoter. The second TU includes
149 the HDV-*X-tra* expression regulated by the TRE promoter. In this setup, Dox can be used to modulate
150 the amount of burden imposed, similar to what was already shown in **Fig. 2b**.

151 We compared this circuit to a catalytically inactive mutant of the HDV ribozyme. As expected,
152 we observed that when the HDV ribozyme is inactive, *X-tra* protein levels increase with decreasing
153 amounts of Dox (**Supplementary Fig. 10, top pale pink bar**), whereas those of the *capacity monitor*
154 decrease (**Fig. 2e, bottom pale blue bar**). In contrast, when the HDV ribozyme is active, *X-tra*
155 expression is strongly reduced and only minorly increasing with lower Dox concentrations
156 (**Supplementary Fig. 10, top dark purple bar**). Here, the *capacity monitor* levels decrease to a
157 smaller extent than in the previous condition, supporting the observations in **Fig. 2c** that
158 transcriptional resources are limited to a certain extent (**Fig. 2e, dark blue bar**). Interestingly, the
159 expression levels of the *capacity monitor* with active HDV ribozyme are higher compared to the
160 inactive mutant (**Supplementary Fig. 10, bottom dark blue bar**). We suggest that, assuming that the

161 *X-tra* mRNA with an active HDV ribozyme is decapped and rapidly degraded, it is likely to sequester
162 fewer translational resources, which should result in higher expression of the *capacity monitor*.
163 Transcriptional resource pool sharing is therefore at least partially responsible for the
164 described gene expression trade-offs, and translational resources may represent an additional
165 bottleneck to the overall expression of synthetic genes. We confirmed this hypothesis by adding a
166 synthetic intron[27] in the 5'UTR of the *X-tra* fluorescent protein (**Fig. 2f, top**). The synthetic intron
167 enhances translation by augmenting mRNA export from the nucleus to the cytoplasm[27] and therefore
168 imposes specific translational load. Indeed, we observed higher expression of *X-tra* in H1299,
169 HEK293T, HeLa, and U2OS cell lines in the presence of a synthetic intron, accompanied by lower
170 *capacity monitor* levels (**Fig. 2f**, **Supplementary Fig. 11**), confirming that resources employed for
171 translational regulation are also limiting. Thus our data collectively indicate that exogenous genes
172 compete for resources both at the transcriptional and translational levels, overall imposing a gene
173 expression burden on mammalian cells.
174 Since one of the goals in synthetic biology is output predictability, reproducibility and
175 robustness, gene expression burden is a key issue to address. We reasoned that post-transcriptional
176 and translational regulators, such as RBPs and miRNAs, may free up cellular resources[28] by repressing
177 target mRNA translation or inducing its degradation. If true, they could be exploited in more robust
178 circuit topologies to reduce gene expression load, resulting in improved performance and
179 predictability of engineered circuits. Therefore, we tested two RBPs, L7Ae and Ms2-cNOT7[29,30] (**Fig.
180 2g, Supplementary Fig. 12-13**), as well as endogenous miRNAs, miR-31, miR-221 and miR-21 (**Fig.
181 2h**). For each system, a fluorescent protein encoding mRNA targeted by either RBPs or miRNAs
182 (*X-tra*) was co-expressed with a second, constitutively expressed fluorescent readout (*capacity
183 monitor*). L7Ae binds the 5'UTR of the *X-tra* mRNA inhibiting its translation, whereas Ms2 binds
184 target sites in the 3'UTR of the *X-tra* transcript, allowing cNOT7 to cut the polyA tail to destabilize the
185 target mRNA[29]. We tested the systems in U2OS, H1299, HEK293T and HeLa cell lines, and consistently
186 observed that *X-tra* downregulation by RBPs results in increased levels of the *capacity monitor* (**Fig.
187 2g, Supplementary Fig. 12-13**).
188 miRNAs operate by either translation inhibition or mRNA degradation, according to
189 complete[31] or partial[32] complementarity to the mRNA target. To evaluate the effect of miRNA
190 regulation on cellular resources re-allocation, we placed three perfect complementary target sites
191 (TS) in the 3'UTR of *X-tra*, which respond to the endogenous miR-31, miR-221, miR-21, highly
192 expressed in H1299, U2OS, and HeLa cells respectively. The *capacity monitor* expression levels
193 increased when the *X-tra* mRNA was downregulated by miRNAs, as compared to controls lacking
194 miRNA target sites (**Fig. 2h**).

195 Due to their high productive capability[33], CHO-K1 cells are the workhorses of the
196 biopharmaceutical industry and have been extensively engineered to favor the expression of
197 therapeutic proteins with desired post-translational modifications. We demonstrate that burden also
198 affects these cells either by increasing *X-tra* gene amounts or enhancing its translation
199 (**Supplementary Fig. 14a,b**). Redistribution of resources is also observed via regulation by the RBP
200 L7Ae and the highly expressed endogenous miR-21 (**Supplementary Fig. 14c,d**).
201 These results confirm that post-transcriptional regulators can redistribute intracellular
202 resources and importantly, that this phenomenon is cell-context independent. The extent of negative
203 correlation between *X-tra* and *capacity monitor* expression, as well as the amount of repression by
204 post-transcriptional regulators differs across cell lines; this could be the consequence of several
205 factors, such as the relative abundance of transcriptional, post-transcriptional and translational
206 resources.
207 A major advantage of miRNAs over RBPs is that they are endogenously expressed and
208 cell-line specific. Thus, their expression does not impose an additional burden, and since several
209 thousand endogenous miRNAs with different target sites are naturally present in mammalian cells [34],
210 the design space is rather large, giving rise to a tremendous number of circuits that can be easily
211 tailored to the cell/tissue of interest. Based on the results presented here, we envision that genetic
212 circuits that mitigate resource competition via miRNAs may be designed for any mammalian cell line
213 with a very broad set of potential applications.

214 **Characterizing the effect of miRNAs on resource distribution**

215 We sought to characterize the correlation between miRNA-mediated downregulation and resource
216 redistribution, by building a library of *miRNA sensors* for miR-31, which is endogenously expressed in
217 H1299 lung cancer cells[35]. The *miRNA sensor* is composed of the fluorescent reporter mKate with or
218 without miR-31 TS, encoded along with the *capacity monitor* (EGFP) on a single plasmid with a
219 bidirectional promoter (**Fig. 3a**). The library includes 0, 1, or 3 fully complementary miR-TS in the 3'
220 or 5'UTR of mKate.
221 Similar to what was previously observed (**Fig. 2g**), when the *miRNA sensor's* levels decrease
222 as a consequence of miR-31 regulation, the expression of the *capacity monitor* increases. The
223 strongest repression was achieved with 3TS in the 5'UTR and was accompanied by corresponding
224 higher capacity monitor levels (**Fig. 3b**). Conversely, when we rescued mKate expression by a miR-31
225 inhibitor (**Fig. 3c left, Supplementary Fig. 15 pink bars**), the *capacity monitor* levels decreased (**Fig.
226 3c right, Supplementary Fig. 15 dark blue bars**) demonstrating that miRNA sensor and *capacity
227 monitor* levels are linked. Interestingly, the effect of the miRNA inhibitor was more pronounced with
228 TS placed in the 3'UTR. Synthetic miRNA inhibitors bind to endogenous miRNAs in an irreversible

229 manner[36], but differences in their action (e.g. when target sites are placed in the 3' *vs* 5' UTR), as well
230 as mechanistic insights into these differences, are still missing.
231 To confirm that miRNA-mediated resource redistribution is independent of experimental
232 setting and plasmid design, we encoded the *miRNA sensor* and *capacity monitor* on two separate
233 plasmids. Similar to previous results, *miRNA sensor* and *capacity monitor* were negatively correlated
234 (**Supplementary Fig. 16a**), suggesting that cellular burden and miRNA-dependent resource
235 reallocation are a common challenge and solution respectively. Downregulation of the *miRNA sensor*
236 was also confirmed by qPCR (**Supplementary Fig. 16b**). Finally, when the *miR-31 sensor* was
237 transfected in low miR-31 cell lines such as U2OS and HEK293T, neither the *miRNA sensor* nor the
238 *capacity monitor* levels varied (**Supplementary Fig. 17**), further confirming the miRNA-dependent
239 resource reallocation.
240 We showed in **Fig. 2h** that miRNA-dependent resource reallocation is observed across
241 different cell lines, by expressing cell-specific *miRNA-sensors* which include 3TS in the 3'UTR. We
242 then built a library of sensors with different numbers and locations of TS for miRNA-221 and -21
243 which are highly expressed in U2OS and HeLa cells respectively. We also confirmed here that
244 *miRNA-sensor* and *capacity monitor* are inversely correlated, consistent with our observations in
245 H1299 cells (**Supplementary Fig. 18-19**).
246 Overall these data show that miRNAs can be used to develop resource-aware
247 plasmid-designs harbouring burden-mitigating circuit topologies, and that the number and location
248 of TS can be tuned to achieve desired protein expression levels.

249 **A gene expression model that incorporates shared cellular resources recapitulates unexpected**
250 **dose-response data**
251 In order to provide a better understanding of our results, we developed a general resource-aware
252 model, which offers a simple and convenient framework for extending existing models of
253 biochemical reactions allowing them to incorporate the effects of shared limited resources. This
254 framework follows ideas originally used to capture the competitive interaction of multiple inhibitors
255 with an enzyme[37] and has been applied to describe shared cellular resources in previous
256 studies[15–18,38].
257 **Fig. 4a** illustrates an overview of the framework. The main idea is to replace the rates of
258 reactions that involve a shared resource with an *effective* reaction rate that captures the reduced
259 availability of that resource due to the presence of competing genes. To create a distinction between
260 regular reactions and resource-limited ones, we use double-headed reaction arrows to denote
261 resource-limited reactions as illustrated at the bottom of **Fig. 4a**. This double-headed arrow
262 summarizes the set of intermediate interactions shown in more detail at the top left of **Fig. 4a**. Here,

263 the substrate A_i binds resource R with rate k^+_i to form the complex C_i. This reaction is also assumed to
264 be reversible with rate k^-_i. With a rate k^{cat}_i the complex gives rise to the product B_i, while also freeing
265 up both the substrate A_i and the resource R. We assume that the total amount of resource, R^{total}, is
266 conserved and remains constant at the time scale of the considered reactions. Considering all
267 possible substrates that require resource R and assuming that C_i is in quasi-steady-state, the rate for
268 resource-limited production can be expressed as k^{eff}_i, shown in the top right corner of **Fig. 4a**. k^{eff}_i is a
269 function of the total amount of resources and the current concentration of all substrates competing
270 for this resource. This expression can be readily used to substitute all reaction rates that involve
271 shared and limited resources.

272 In Lillacci *et al.*[22], new synthetic control systems were introduced to enhance the robustness
273 of gene expression. The same study also described a non-monotonic dose-response behavior in a
274 simple inducible gene expression system. Such non-monotonic behavior is rather surprising and
275 seems unintuitive, especially considering that conventional methods of modelling gene expression
276 via Hill-type functions can only produce monotonically increasing (or decreasing) dose-response
277 curves. Although Lillacci *et al.* proposed models for the different circuit topologies[22], the effect of
278 competition for limited resources was not considered. To demonstrate the effectiveness of our
279 modelling framework, we extend these models to include limited resources and show that the
280 resulting extended models recapitulate the experimental observations.

281 The four topologies considered in Lillacci *et al.*[22] were split into two groups based on the
282 presence of negative feedback from the fluorescent protein DsRed to the transcriptional activator
283 (tTA). The first group consisted of the open-loop (OLP) and incoherent feedforward (IFF) topologies.
284 In both these circuits, the constitutively expressed transcriptional transactivator, fused to the
285 fluorescent protein Cerulean (tTA-Cer), activates the expression of the fluorescent protein DsRed.
286 Furthermore, the gene of DsRed intronically encodes the synthetic microRNA FF4 (miR-FF4). In the
287 IFF topology, the matched target of this microRNA is present in the 3' untranslated region (UTR) of
288 the DsRed gene. This target is replaced by a mismatched target for the microRNA FF5 in the OLP.
289 These detailed interactions are depicted here in **Fig. 4b left side**. To observe potential shifts in the
290 allocation of resources, we generated dose-response curves by increasing the amount of transfected
291 tTA-Cer plasmid, while the other two plasmids, containing DsRed and the constitutively expressed
292 fluorescent transfection reporter mCitrine, were held constant. As can be seen from the model fit,
293 plotted as a solid line in the data graph, the extended model reproduces the non-monotonic
294 behavior of the dose-responses (**Fig. 4b, right**).

295 The second group of topologies considered by Lillacci *et al.* consisted of the feedback (FBK)
296 and the FBK+IFF hybrid (HYB) topologies. In addition to all the interactions described for the OLP and
297 IFF circuits, the FBK and the HYB circuits possess miR-FF4 targets in the 3' UTR of the tTA-Cer gene,

298 which introduces negative feedback. Furthermore, the FBK and HYB differ from each other by the
299 presence of a matched target for miR-FF4 in the HYB topology, which introduces incoherent
300 feedforward and is replaced by a mismatched FF5 target in the FBK circuit. All the interactions are
301 illustrated in detail in **Fig. 4c, left**. The dose-response curves for the two circuits were obtained as
302 described above. Again, the fit of the extended model to the data captures its rather unexpected
303 behavior (**Fig. 4c, right**).
304 Our simple framework adapts existing models of gene expression to include pools of shared
305 and limited resources. We show that it can be used to provide an explanation for unintuitive
306 dose-responses in tTA-based circuits. With this framework as a tool, we believe that performance
307 issues attributed to gene expression burden can be addressed head-on in the design phase of
308 circuit-building, thereby reducing the need for costly subsequent build-test-learn iterations.

309 **Mitigating cellular burden with Incoherent Feed-Forward Loop (iFFL) circuits**
310 We implemented a strategy that exploits miRNA to reduce the indirect coupling between
311 co-expressed genes. In particular, we took advantage of the fact that miRNA production also requires
312 (pre-translational) cellular resources, therefore acting as a sensor for resource availability. Because of
313 this, it is possible to reduce the coupling between genes co-expressed via a common resource pool
314 by introducing miRNA-mediated repression of those genes (as long as the miRNA itself is also
315 affected by the same resource pool). Since both the miRNA and the miRNA-repressed gene are
316 affected by the availability of resources, miRNA-mediated repression implements an incoherent
317 feedforward loop similar to previously published circuits[22,25,39] (**Fig. 5a**). Interestingly, this iFFL-based
318 circuit constitutes a biological implementation of the miRNA circuit proposed by Zechner *et al*[40]. In
319 this setting, the miRNA can be interpreted as an estimator of its cellular context (e.g. amount of free
320 resources) and acts to filter out this context, thereby minimizing its impact on the output of interest.
321 We explored this strategy for an endogenously expressed miRNA (**Fig. 5b,c**) and a synthetic
322 miRNA encoded on a plasmid (**Fig. 5d,e**). More specifically, **Fig. 5b** describes a strategy that exploits
323 endogenous miRNAs to reduce the coupling of a gene of interest (GOI) to the expression level of
324 other genes, introduced by the limitation in resources. Implementation of this strategy only requires
325 adding target sites of an endogenous miRNA to the 5' UTR of the gene of interest (mKate). In our
326 experimental setup, when the copy number of a second gene *(X-tra)* is increased, resources are
327 drawn away from the expression of mKate and allocated to the expression of *X-tra*. The shift in
328 resource allocation is expected to also affect the miR-31, which acts as a *capacity monitor*. This leads
329 to a reduction in the repression of mKate, effectively compensating for the burden imposed by the
330 co-expression of the *X-tra* gene.

To demonstrate this mitigation approach experimentally, we co-transfected H1299 cells with increasing amounts of EGFP (*X-tra*), along with a constant amount of mKate (*GOI*) that either includes (for mitigation) or omits (no mitigation) three miR-31-TS in the 5'UTR. As expected, the expression level of *X-tra* approached saturation as the plasmid copy number increased, both for the targeted and non-targeted *GOI* variants (**Fig. 5c**). In agreement with previous results, the expression of the non-targeted *GOI* strongly decreased with increased expression of *X-tra*. Conversely, the decrease in expression of the targeted *GOI* was only about a third of that of the non-targeted variant, indicating improved adaptation to changes in resource availability (**Fig. 5c, Supplementary Fig. 20**). This observation was also captured well by a model of the system that explicitly considered resources, as described in the previous section. Analogously, miR-221-iFFL circuits specific for U2OS (**Supplementary Fig. 18)** and HEK293T cells[41] (**Supplementary Fig. 22**) show improved robustness to burden imposed by increasing exogenous gene load (**Supplementary Fig. 21, 23**).

Importantly**,** the delivery of genetic payloads also affects the expression of endogenous genes (CyCA2, eIF4E and GAPDH), as shown in **Fig. 2d**. We then sought to compare the expression of the same endogenous genes in the presence or absence of miR-31 sensor in H1299 cells. After 48h from transfection of EGFP and mKate on a bidirectional plasmid, with mKate either including (miRNA sensor) or not (noTS) target sites for miR-31, we sorted cells according to high, intermediate or absence of fluorescence expression (**Supplementary Figure 24a**) and performed qPCR. Curiously, we observed that in cells transfected with miR-31-sensor, the decrease in the expression of the endogenous genes was much lower than in its absence (**Supplementary Figure 24c**). Furthermore, the expression of endogenous genes was inversely proportional to the levels of fluorescent proteins (**Supplementary Figure 24b**). Thus, the lower expression of endogenous genes due to the burden imposed by exogenous payloads is counteracted by the miR31-sensor.

Motivated by our desire to achieve portability across cell lines and multiple-output regulation are desired features of synthetic devices, we implemented and tested a synthetic miRNA-iFFL circuit that tunes three GOIs (**Fig. 5d**). Similar to the endogenous case, the genes-of-interest, mCitrine (GOI_1) and mRuby3 (GOI_2), encode target sites for the miRNA-FF4 in their 3' UTRs. In contrast to endogenous miRNA expression, however, here the miRNA is expressed intronically from GOI_2. In this way, the circuit forms a self-contained unit that can be easily transferred between cell types.

We co-transfected HEK293T cells with a plasmid encoding constitutively expressed miRFP670 (*X-tra*) and a plasmid composed of two transcriptional units (TU), each expressed under the constitutive promoter EF1α (**Fig. 5d**). The first TU encodes the mCitrine, whereas the second drives mRuby3. Furthermore, the 3' UTR of mRuby3 contained either three target sites for the synthetic miRNA-FF4 or three mismatched miR-FF5 target sites (negative control). The miRNA-FF4 was

366 intronically encoded in the mRuby3 gene. Identically to the endogenous case, the amount of *X-tra*
367 plasmid was increased while keeping the *GOIs'* plasmid constant. Again, expression of *X-tra* increased
368 and approached saturation with increasing molar amounts and consequently, the non-targeted
369 variants of the *GOIs* decreased (**TFF5 in Fig. 5e**). Conversely, the expression of the targeted variants
370 (**TFF4 in Fig. 5e**) decreased to a lesser extent than the non-targeted ones, analogously to what was
371 observed for endogenous miRNAs, albeit with lower efficiency. Finally, to demonstrate the portability
372 of the device we tested the approach in mouse embryonic stem cells (**Supplementary Fig. 25**). Here,
373 adaptation to shifts in resource availability was similar to the endogenous miRNA-based regulation
374 (**Fig. 5d**). Thus, we showed that also in entirely synthetic systems, adaptation to shifts in resource
375 availability was achieved. To ensure that the observed mitigation was not caused by a higher
376 tolerance to changes in availability at lower expression levels, we showed analytically using the
377 described modelling framework that the normalized expression at lower levels was more sensitive to
378 burden (**Supplementary Note 2**).
379 Overall, these results suggest that our approach can be used to mitigate resource-mediated
380 coupling of gene expression despite cell-to-cell variability, demonstrating the portability and broad
381 applicability of our findings. Our results demonstrate that iFFL circuits can mitigate burden from
382 transgene expression in mammalian cells. Importantly, by using miRNA one can either opt for
383 endogenous miRNAs to specifically tailor a circuit to a desired cell line, or create a portable circuit by
384 using a synthetic miRNA such as miR-FF4.

385 Discussion

386 Our study demonstrated for the first time that the sharing of limited cellular resources represent a
387 general bottleneck for the predictability and performance of synthetic circuits in mammalian cells,
388 with important consequences for mammalian synthetic biology, molecular biology, as well as for
389 biotechnology applications. We showed that heterologous gene expression imposes a resource
390 burden, independent of cell type (six different cell lines were tested) and of promoter strength (**Fig.
391 2a,b, Supplementary Fig. 1,5-6**), although it is more severe with high plasmid copy number (**Fig. 2a**).
392 Further, we presented a detailed characterization of the distinct contributions of
393 transcriptional and translational burden by combining molecular biology techniques (**Fig. 2c-d**) with
394 the engineering of simple genetic motifs that enabled the specific control of translation of the
395 desired gene (**Fig. 2e,f**). Notably, we showed that endogenous and synthetic post-transcriptional and
396 translational regulators such as RNA-binding proteins and miRNAs can effectively redistribute cellular
397 resources (**Fig. 2g,h-3**), an observation we exploited to engineer resource-aware synthetic circuits
398 that utilize post-transcriptional regulation to mitigate burden.

We showed that endogenous genes are also affected by the burden imposed by genetic payloads (**Fig. 2d**), whereas this effect was less pronounced in the presence of the miRNA sensor (**Fig. 3a middle, Supplementary Fig. 24c**). We speculate that this positive effect of miRNA sensor is attributed to the freeing up of translational resources, leading to the increase of proteins involved in the transcription of endogenous genes. At the same time, as already proposed in *Gambardella et al.*[42], the downregulation of mKate by miR-31 may lead to a 'queueing effect' for the degradation of the other mRNAs, similar to what was shown with two independent proteins tagged for degradation by the proteasome[43].

To get a deeper understanding of the mechanisms through which resource sharing dynamically couples gene expression and to explain resulting non-intuitive behavior of genetic circuits induced by such coupling in mammalian cells[22], we described a modelling framework that captured the indirect interdependence of gene expression in a resource-limited context. Our framework for introducing resource-limited reactions into pre-existing models of synthetic circuits provides a straightforward way of obtaining resource-aware models and facilitates the design of circuits that are less prone to burden effects. For instance, the family of controllers analyzed in **Fig. 4** exemplifies the non-intuitive behavior that might arise due to burden. Here, limiting resources led to a non-monotonic dose-response in a simple transcription factor and reporter pair. Our extended modelling framework successfully captured this unexpected behavior of the dose-responses (**Fig. 4b**), which could not be explained by traditional models. This same modelling framework suggested that an incoherent feedforward loop (iFFL) is a particularly well-suited circuit motif for mitigating burden effects. The incoherent feedforward loop (iFFL) itself is one of the core gene regulatory motifs in biology, and unsurprisingly it has served as inspiration for many synthetic genetic circuits that exploit its adaptation properties, particularly to input perturbations[22,25,39,44]. This together with our experimental observations on the effective role of miRNA in resource distribution (**Fig. 2h, 3**) led us to choose a specific implementation of this motif based on miRNAs for burden mitigation in mammalian cells (**Fig. 5**).

Given its importance in synthetic circuits, resource burden has recently been studied in *E. coli*[12,16,19,20], where two different synthetic circuits have been used for burden mitigation. In Ceroni *et al.*[20], the mitigation strategy aims to reduce the expression of the gene of interest to avoid burden, while the strategy in Huang *et al.*[19] aims to maintain the expression of a gene of interest upon a reduction of resources, possibly at the expense of other genes. Both strategies rely on negative feedback, a regulatory circuit motif that is widely used in natural and synthetic circuits. While iFFL is also a common regulatory motif, iFFL circuits have not to date been utilized in burden mitigation, in spite of several distinct advantages over negative feedback circuits for burden mitigation. In particular, iFFL circuits are considerably simpler to implement and much easier to tune than negative

434 feedback circuits, which usually require more components and can become dynamically unstable if
435 not properly designed and tuned. In terms of dynamic response, iFFL circuits are also generally faster
436 in rejecting disturbances like a sudden change in resource availability. Indeed iFFL regulation
437 responds to the disturbance itself, while negative feedback begins to act only after the impact of the
438 disturbance on the regulated output has been detected.

439 In mammalian cells, burden-mitigating circuits have not been proposed until *this* and
440 another accompanying study by Jones *et al.*[45] (Nature Biotechnology joint submission). While both
441 studies independently reached the conclusion that iFFL motifs are ideally suited for burden
442 mitigation in mammalian cells, the two studies follow complementary paths for the circuit
443 implementation of this motif, with both implementations successfully demonstrated in multiple cell
444 lines. In the Jones *et al.* study, an endoribonuclease-based iFFL is used to mitigate the effects of
445 resource burden. While the use of RNA-binding proteins to implement iFFL circuits in mammalian
446 cells is not new[46], the use of endoRNAse for load mitigation in Jones *et al.* was not previously
447 reported. One feature of RNA-binding protein iFFL circuits is that they do not rely on other factors
448 like RISC for their function. Another feature of RNA binding protein mitigation implementations is
449 that they respond directly to changes in translational resources, even though they were designed for
450 transcriptional resource mitigation.

451 In this study we adopt a miRNA implementation of iFFL circuits for the purpose of burden
452 mitigation. miRNA-iFFLs have been demonstrated to increase robustness to gene dosage
453 variability[22,44] and gene expression noise[25,39], but their use for burden mitigation in any cell type is
454 novel. After considering both RNA-binding proteins (L7Ae and Ms2-cNOT7) and miRNA for iFFL
455 implementations (**Fig. 2g,h**), we opted for a miRNA-based one (both endogenous and synthetic) due
456 to several considerations. Importantly, miRNA circuits do not use genetic components that derive
457 from different organisms, circumventing potential toxicity and immunogenicity concerns that could
458 limit their application in medical therapy[47,48]. Additionally, as we highlight next, miRNA-iFFLs exhibit
459 high versatility, faster dynamics[49], and other distinctive features that are important for
460 biotechnological applications.

461 To date, endogenous miRNA have been used as inputs to synthetic cell type classifier
462 circuits[50,51] but their use as incoherent feedforward signals is unprecedented and provides important
463 advantages over protein-based implementations. Specifically, iFFL circuits that exploit endogenous
464 miRNAs do not require the expression of additional components (no additional translational burden
465 is imposed), enable cell-type *specificity*[50,52] and can enhance stabilization against perturbation by
466 inserting target sites for one or more endogenous miRNAs (*scalability*). At the same time, synthetic
467 miRNAs enable *portability* of circuits across different cell lines, and the flexibility at the sequence
468 level allows scaling up to many orthogonally operating circuits. Additionally, synthetic miRNA-based

469 iFFLs are compact and can be easily included in pre-existing genes as introns containing the miRNA
470 scaffold (*minimal footprint* on the transcriptional resources of the cell), making them suitable for
471 therapeutic applications such as gene therapy. For example, while protein-based iFFLs require
472 incorporation of much longer sequences, miRNA-based iFFL could be used in AAV-mediated gene
473 therapy because their smaller sequences well fit within the maximum cargo capacity of 4.5 kb of AAV
474 vectors[53].

475 Another critical feature of miRNAs is their *programmability*. The specificity of a miRNA can
476 be easily engineered to target any synthetic or endogenous gene without the need to engineer the
477 target itself[54–56]. This again has implications for medical applications, where the target might not be
478 accessible for modification. One possible limitation here is that the use of the same miRNA to
479 regulate multiple targets might lead to depletion of the miRNA, giving rise to an inevitable trade-off.
480 This trade-off is observed for competing endogenous RNA (ceRNA), which are known to naturally
481 regulate other RNAs by competing for miRNA-binding. The principle of ceRNA has been
482 demonstrated synthetically on a gene circuit[57]. Finally, *tunability* of repression strength can be easily
483 achieved both through the number and the placement of the targets (**Fig. 3**). Such tunability of
484 repression can be used to enhance adaptation to variations in resource availability. It should be
485 noted that stronger repression will yield lower expression levels of the gene of interest. This tradeoff
486 is unavoidable, and inherent to all implementations of iFFL burden mitigation circuits, including
487 endoRNase implementations.

488 In terms of burden mitigation, at first thought one might argue that miRNA-based iFFL would
489 only mitigate coupling through shared resources on the transcriptional level since translational
490 resources do not affect miRNA production. However, given that several proteins are involved in the
491 maturation, transportation, and activity (e.g. RISC multi-protein) of miRNAs and these proteins are
492 impacted by translational resource availability, this would indirectly allow miRNA-based iFFLs to also
493 mitigate translational burden. In any case, translational burden mitigation may be easily incorporated
494 *directly* by expressing the miRNA under the control of a synthetic or endogenous transcription factor.
495 Implementation considerations aside, we point out that due to the differences and unique features
496 of both miRNA and endoRNase implementations, we expect that in the future it will be desirable to
497 combine them in single cells to create an even larger set of simultaneously operating
498 burden-mitigating circuits.

499 Understanding the impact of resource availability will have important consequences for
500 biological studies and for improved mammalian cell engineering. For example, for successful
501 treatment, cell therapies that rely on the fine expression and secretion of therapeutic molecules can
502 now be designed with resource-aware circuits. Our findings suggest that, when choosing a host cell
503 line, one of the key factors to consider should be its transcriptional and translational capacity[21], not

504 only in terms of productivity, but also in terms of the ability of the cells to maintain their fitness over
505 the production phase. In this respect, enhancing the insulation of synthetic genetic circuits from
506 cellular metabolism is paramount. In our study, we implemented a system that could efficiently
507 sustain the production of up to three (and probably more) output proteins (**Fig. 5**), reducing the
508 unwanted coupling among their expression levels and with other cellular processes. However, it
509 should be noted that our system was not intended to reach the highest expression levels, as its
510 purpose was instead to allow the concurrent production of several output proteins in a predictable
511 manner.

512 Finally, studies of biological functions that employ system perturbations by exogenous gene
513 expression often lack accuracy and exhibit highly variable results due to less-than-optimal genetic
514 circuit designs. This is critical when performing quantitative analyses, for which predictability and
515 reproducibility are essential. Our study presents a portable design capable of enhancing the
516 insulation of transgene expression and will thus contribute to the development of robust-by-design
517 mammalian synthetic circuits, with important implications for basic science and applications in
518 industrial biotechnology and medical therapy.

519 Methods

520 **Cell culture**. HEK293T, U2OS and HeLa cells (ATCC) used in this study were maintained in
521 Dulbecco's modified Eagle medium (DMEM, Gibco); H1299 were maintained in Roswell Park
522 Memorial Institute medium (RPMI, Gibco); CHO-K1 were maintained in Minimum Essential Medium
523 α (α-MEM, Gibco). All media were supplemented with 10% FBS (Atlanta BIO), 1%
524 penicillin/streptomycin/L-Glutamine (Sigma-Aldrich) and 1% non-essential amino acids (HyClone).
525 HEK239T cells (ATCC, strain number CRL-3216) used for part of this study were maintained in DMEM
526 (Sigma-Aldrich or Gibco) supplemented with 10% FBS (Sigma-Aldrich), 1X GlutaMAX (Gibco) and 1
527 mM Sodium Pyruvate (Gibco). E14 mouse embryonic stem (mES) cells were grown in DMEM (Gibco)
528 supplemented with 15% FBS (PAN Biotech; specifically for ES cell culture), 1% penicillin/streptomycin
529 (Sigma-Aldrich), 1% non-essential amino acids (Gibco), 2 mM L-Glutamine (GlutaMAX; Gibco), 0.1
530 mM beta-mercaptoethanol (Sigma-Aldrich) and 100 U/mL Leukemia inhibitory factor (LIF;
531 Preprotech). At every passage the media was additionally supplemented with fresh CHIR99021 to 3
532 uM and PD0390125 to 1 uM to support naïve pluripotency (2i conditions[58]). All labware used was
533 coated with 0.1% gelatin (prepared ourselves) prior to plating the ES cells. The cells were maintained
534 at 37 °C and 5% CO2.

535 **Transfection**. Transfections were carried out in 24-well plate for flow cytometry analysis or in
536 a 12-well plate format for flow cytometry and qPCR analysis run on the same biological replicates
537 (**Supplementary Table 1**). Transfections for **Fig. 2d** and **Supplementary Fig. 8** were carried out in 6
538 cm dishes. H1299, HeLa, U2OS, HEK293T and CHO-K1 cells were transfected with Lipofectamine®
539 3000 (ThermoFisher Scientific) according to manufacturer's instructions and 300 ng total DNA (500
540 ng in **Fig. 2c,d** and **Supplementary Fig. 1-5,8,9**) in 24-well plates. DNA and transfection reagents were
541 scaled up according to the Lipofectamine® 3000 manufacturer's instructions. miR-31 inhibitor
542 (Invitrogen™ *mir*Vana™ miRNA Inhibitors) was cotransfected using the same method as for DNA (**Fig.**
543 **3c**).
544 HEK293T cells used for experiments shown in **Fig. 2a,b,e, 4** and **5e** were plated
545 approximately 24h before transfection at 62500 to 75000 cells per well in 24-well plates. The
546 transfection solution was prepared using Polyethylenimine (PEI) "MAX" (Mw 40000; Polysciences,
547 Inc.) in a 1:3 (ug DNA to ug PEI) ratio with a total of 500 ng of plasmid DNA per well. Both DNA and
548 PEI were diluted in Opti-MEM I reduced serum media (Gibco) before being mixed and incubated for
549 25 minutes prior to addition to the cells. E14 mouse embryonic stem cells were transfected using
550 Lipofectamine® 2000 (ThermoFisher Scientific) in a 1:3 (ug DNA to ug Lipofectamine® 2000) with 300
551 ng of plasmid DNA per well. The transfection was performed on cells in suspension immediately after
552 plating at approximately 30000 cells per well. All wells were coated with 0.1% Gelatin before the
553 addition of the cells.

554 **Flow cytometry and data analysis**. H1299, HEK293T, U2OS, HeLa and CHO-K1 cells were
555 analyzed with a BD Facsaria™ cell analyzer (BD Biosciences) or BD Celesta™ cell analyzer (BD
556 Biosciences) using 488 and 561 lasers. For each sample >20000 singlet events were collected and
557 fluorescence data were acquired with the following cytometer settings: 488 nm laser and 530/30 nm
558 bandpass filter for EGFP, 561 nm laser and 610/20 nm filter for mKate. Cells transfected in 12-well
559 plates were washed with DPBS, detached with 100 µL of Trypsin-EDTA (0.25%) and resuspended in
560 600 µL of DPBS (Thermo Fisher). 200 µL of cell suspension were used for flow cytometry and 400 µL
561 for RNA extraction. HEK293T used for experiments shown in **Fig. 2a,b,e, 4** and **5e** cells were
562 measured 48 hours after transfection on a BD LSRFortessa™ Special Order and Research Product
563 (SORP) cell analyzer. mCitrine fluorescence was excited via a 488 nm laser and was detected through
564 a 530/11 nm bandpass filter. mRuby3 was excited via 561 nm laser and measured through a 610/20
565 nm bandpass filter. miRFP670 was excited at 640 nm and measured through a 670/14 nm bandpass
566 filter. E14 mES cells were measured 48 hours after transfection on a Beckman Coulter CytoFLEX S
567 flow cytometer. mCitrine fluorescence was excited using a 488 nm laser and was detected through a
568 525/40+OD1 bandpass filter. mRuby3 was excited with 561 nm laser light and measured through a

569 610/20+OD1 bandpass filter. miRFP670 was excited at 638 nm and measured through a 660/10
570 bandpass filter. The cells were collected for measurement by washing with DBPS (Sigma-Aldrich or
571 Gibco) and detaching in 70 to 180 µL of Accutase solution (Sigma-Aldrich). For each sample between
572 10000 to 200000 singlet events were collected. Fluorescence intensity in arbitrary units (au) was
573 used as a measure of protein expression. For each experiment a compensation matrix was created
574 using unstained (wild type cells), and single-color controls (mKate/mCherry only, EGFP only or
575 mCitrine only, mRuby3 only, miRFP670 only). Live cell population and single cells were selected
576 according to FCS/SSC parameters (**Supplementary Fig. 26, 27**). Data analysis was performed with
577 Cytoflow or a custom R script. Data fitting was performed using Mathematica's NonlinearModelFit
578 function and the InteriorPoint method.

579 **Cell sorting.** H1299 cells used for the experiment shown in **Fig. 2d** were trypsinized from 6
580 cm dishes and counted. They were then centrifuged at 500 g for 5 min and resuspended at a
581 concentration of 5 mln/mL in sorting buffer (PBS 1x + 3 mM EDTA + 0.8 % Trypsin + 1 % FBS). Cells
582 were sorted with a BD FACSMelody™ cell sorter according to their fluorescence levels
583 (**Supplementary Fig. 8**). 150,000 cells per gate were collected.

584 **DNA cloning and plasmid construction.** Plasmid vectors carrying gene cassettes were created
585 using In-Fusion HD cloning kit (Clonetch), Gibson Assembly, via digestion and ligation or using the
586 yeast toolkit (YTK)[59] with custom parts for mammalian cells. Gibson Assembly master mixes were
587 created from Taq DNA Ligase (NEB), Phusion High-Fidelity DNA Polymerase (NEB) and T5 Exonuclease
588 (Epicentre) in 5X isothermal buffer (**Supplementary Table 6**). Ligation reactions were performed in
589 1:2-5 molar ratios of plasmid backbone:gene insert starting with 50 to 100 ng of vector backbone
590 digested with selected restriction enzymes. Assemblies using the YTK were performed according to
591 the original publication[59]. Newly created constructs were transformed into XL10-Gold or TOP10 *E. coli*
592 strains.
593 For plasmids with miRNA target sites, the target sequences were selected using miRBase
594 database (http://www.mirbase.org/) and are listed in **Supplementary Table 4**. List of oligos used to
595 clone endogenous miRNAs TS are listed in **Supplementary Table 3**. All plasmids were confirmed by
596 sequencing analysis and deposited to addgene.
597 To perform western blot analysis, a His-tag composed of 6 Histidine residues was inserted
598 after the start codon of mKate encoding plasmids.

599 **mRNA extraction and reverse transcription.** RNA extraction was performed with E.Z.N.A.®
600 Total RNA Kit I (Omega Bio-tek). The protocol was followed according to manufacturer's instructions
601 and RNA was eluted in 30 µL of RNAse free water. RNA samples were conserved at -80°C.
602 PrimeScript RT Reagent Kit with gDNA Eraser – Perfect Real Time (Takara) was used according
603 to manufacturer's instructions. The protocol was performed on ice in a RNAse free environment to
604 avoid RNA degradation. A negative control without PrimeScript RT Enzyme Mix I was always prepared
605 to investigate genomic DNA contamination.

606 **qPCR**. Fast SYBR Green Master Mix (ThermoFisher Scientific) was used to perform qPCR of
607 cDNAs obtained from 500 ng of RNA and diluted 1:5. Samples were loaded in MicroAmp™ Fast
608 Optical 96-Well Reaction Plate (0.1 mL) and the experiment was carried out with a CFX96 Touch
609 Real-Time PCR Detection System (BioRad) machine. Each well contained 20 µL of final volume (7 µL
610 SYBR Green Master Mix, 10 µL ddHO, 1 µL of each primer, 1 µL of template). Also, a control without
611 template (blank) was set. Primers were designed to amplify a region of 60-200 bp (**Supplementary**
612 **table 5**) and with a temperature of annealing between 50 and 65 °C 72. Data were analysed using the
613 Comparative Ct Method according to Applied Biosystems Protocols.

Acknowledgements

We thank Dr. Gabiele Lillacci for sharing the plasmids expressing the synthetic circuit topologies as well as the plasmid expressing mCitrine, Dr. Maaike Welling for sharing the mES E14 cell line. We thank Daniela Perna and Luca Giorgio Wanderlingh for their technical support. GB.S. gratefully acknowledges support from his UK EPSRC Fellowship for Growth in Synthetic Biology (EP/M002187/1) and his UK Royal Academy of Engineering Chair in Emerging Technologies for Engineering Biology.

Author contributions

T.F., F.C., GB.S., M.K. and V.S. conceived the project. F.C. designed and performed experiments and performed data analysis of endogenous miRNAs, RBPs, transcriptional and translational burden, endogenous genes' expression. T.F. designed and performed experiments and performed data analysis of synthetic miRNA, generic and transcriptional burden (HDV). T.F. and J.G. developed the mathematical model. F.T. and F.C. performed and analyzed iFFL experiments with endogenous miRNAs. M.K. and V.S. supervised the experimental work and secured funding. M.K. and GB.S. supervised the computational work. T.F., F.C., GB.S., M.K., and V.S. wrote the manuscript. All authors edited the manuscript.

Competing Interests statement

The authors declare no competing interests.

Data availability

All relevant data are included as Source Data and/or are available from the corresponding author on reasonable request. Plasmid sequences are deposited on AddGene and GenBank under the accession codes specified in **Supplementary Table 2**. Strains and plasmids used in this study are available from the corresponding author on reasonable request.

Code availability

The code used for automated analysis and fitting is available on reasonable requests from the corresponding authors.

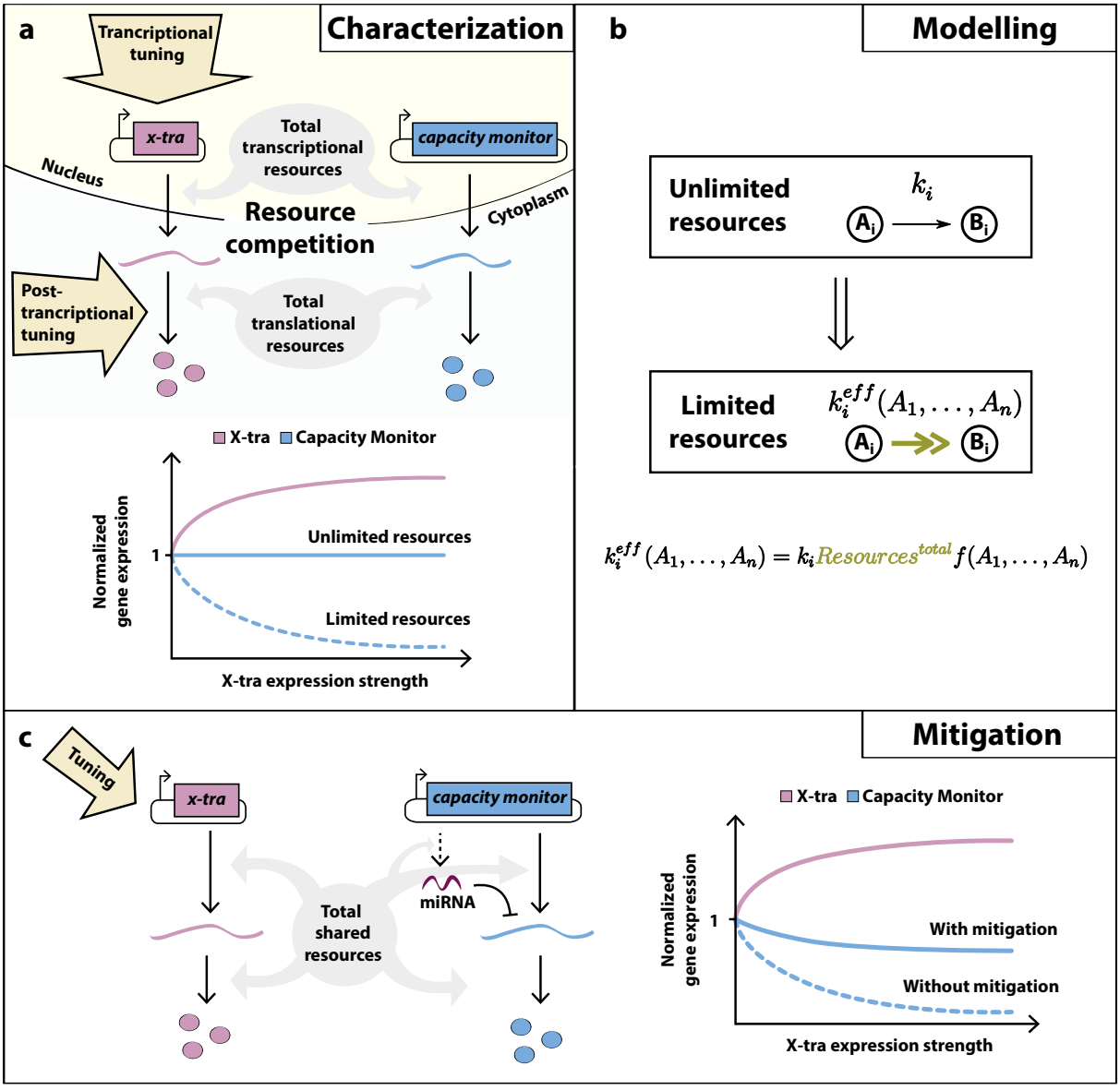

Fig. 1. Graphical abstract. (a) Characterization of gene expression burden. Expression of independent exogenous genes impacts on host cellular resources. Thus, perturbations in one gene's expression (hereby named *X-tra*) affect the expression of a second gene (hereby named *capacity monitor*). **(b) Modelling of gene expression in a resource limited environment.** Modelling of gene expression is generally performed under the assumption of unlimited resources. A simple framework enables the straightforward transformation of such a model to a system that incorporates resources explicitly. The transformation involves a simple function that scales the original reaction rate. **(c) Mitigation of gene expression burden.** A simple microRNA-based circuit motif is capable of mitigating the burden-induced coupling of *X-tra* and the *capacity monitor*.

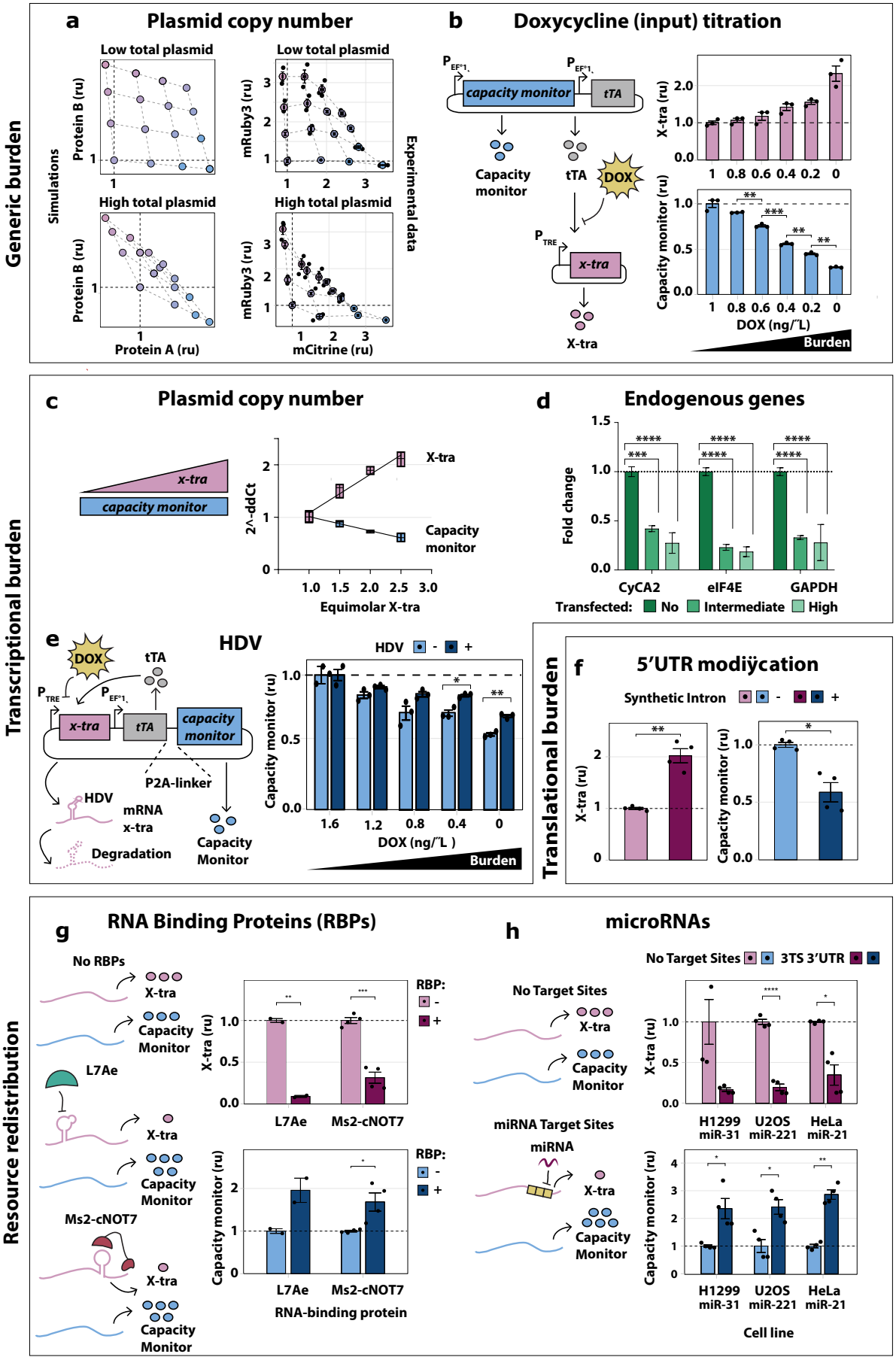
Generic burden
a
Plasmid copy number
Low total plasmid
High total plasmid
Simulations
Experimental data
Protein B (ru)
Protein A (ru)
mRuby3 (ru)
mCitrine (ru)
b
Doxycycline (input) titration
capacity monitor
tTA
Capacity monitor
DOX
x-tra
X-tra
X-tra (ru)
Capacity monitor (ru)
DOX (ng/˝L)
Burden
Transcriptional burden
c
Plasmid copy number
x-tra
capacity monitor
2^-ddCt
X-tra
Capacity monitor
Equimolar X-tra
d
Endogenous genes
Fold change
CyCA2
eIF4E
GAPDH
Transfected:
No
Intermediate
High
e
HDV
DOX
tTA
x-tra
capacity monitor
P2A-linker
HDV
mRNA
x-tra
Degradation
Capacity Monitor
Capacity monitor (ru)
DOX (ng/˝L)
Burden
Translational burden
f
5'UTR modiÿcation
Synthetic Intron
X-tra (ru)
Capacity monitor (ru)
Resource redistribution
g
RNA Binding Proteins (RBPs)
No RBPs
X-tra
Capacity Monitor
L7Ae
Ms2-cNOT7
RBP:
RNA-binding protein
h
microRNAs
No Target Sites
3TS 3'UTR
miRNA Target Sites
miRNA
H1299
U2OS
HeLa
miR-31
miR-221
miR-21
Cell line

649 **Fig. 2. Burden imposed by genetic circuits in mammalian cells. (a)** Left: model-guided simulations
650 accounting for the limited resources (**Supplementary Note 1**) shows the correlation of independent
651 genes' expression. As the total plasmid amount increases, the total protein expression plateaus.
652 Right: Titration of two plasmids constitutively expressing the fluorescent proteins mCitrine and
653 mRuby3 from EF1α promoters in ratios from 1:4 to 4:1, for a total of 50 ng (Top right) or 500 ng of
654 DNA (Bottom right). Computer simulations effectively recapitulate the saturation of gene expression
655 that we observed for a total amount of 50 or 500 ng of plasmids. N=3 biological replicates. **(b)**
656 Inhibition of tTA by Dox treatment further unveils the hidden coupling of expression levels among
657 two genes. Two plasmids were co-transfected, one constitutively expressing *capacity monitor* and tTA
658 from a strong constitutive promoter and the other expressing *X-tra* from a tTA responsive promoter.
659 Data show that *capacity monitor* levels counterbalance the increase in *X-tra* expression. Flow
660 cytometry data are normalized to the expression levels of each gene in absence of Dox. N=3
661 biological replicates. **(c)** Transcriptional burden. mRNA quantification of *X-tra* and a *capacity monitor*
662 expressed at different molar ratios. As the *X-tra* increases, the mRNA levels of the *capacity monitor*
663 decreases. N=4 biological replicates. qPCR analysis was performed 48 hours post transfection and
664 data show fold change +/- SE. **(d)** Cells transfected with a plasmid encoding two fluorescent proteins
665 expressed from a bidirectional promoter were sorted according to *high*, *intermediate* or *no*
666 fluorescence **(Supplementary figure 8)**, and the mRNA was extracted. qPCR shows that the mRNA
667 levels expressed from endogenous genes decrease in cells with *intermediate* and *high* fluorescence.
668 N=3 biological replicates. N=3 biological replicates. Data show fold change +/- SE. **(e)** Increasing the
669 expression of a translationally incompetent mRNA suggest transcriptional burden. *Capacity monitor*
670 levels are higher in the presence of an active HDV ribozyme placed after the start codon of *X-tra*
671 (which results in its rapid degradation of *X-tra*) than in the inactive form, suggesting a sequestration
672 of transcriptional resources. N=3 biological replicates. **(f)** Translational burden. We included a
673 synthetic intron in the 5'UTR of a transcript to increase its translation and to selectively observe
674 translational burden. As expected the synthetic intron shows higher translational load of *X-tra* as
675 compared to the control and leads to reduced *capacity monitor* levels. N=4 biological replicates. **(g)**
676 Post-transcriptional regulators impact translational burden. The RBPs L7Ae and Ms2-cNOT7,
677 downregulate *X-tra* expression by binding the 5' and 3'UTR respectively. Data show that repressed
678 *X-tra* expression leads to increased *capacity monitor* levels. N≥2 biological replicates. **(h)** Similar to (f)
679 also miRNAs reallocate resources by downregulating targeted mRNA which include miRNA target
680 sites (TS) in the 3' UTR. We engineered *X-tra* transcripts with 3TS that respond to either miRNA
681 miR-31, miR-221 or miR-21, endogenously expressed in H1299, U2OS and HeLa cells respectively.
682 Data show that *capacity monitor* levels are higher when the *X-tra* is downregulated by miRNAs. N≥3
683 biological replicates. Flow cytometry data were acquired 48 hours post-transfection and is plotted

+/- SE. SE: standard error. ru: relative units. unpaired T-test. p-value: ****<0.0001, ***<0.0005, **<0.005, *<0.05

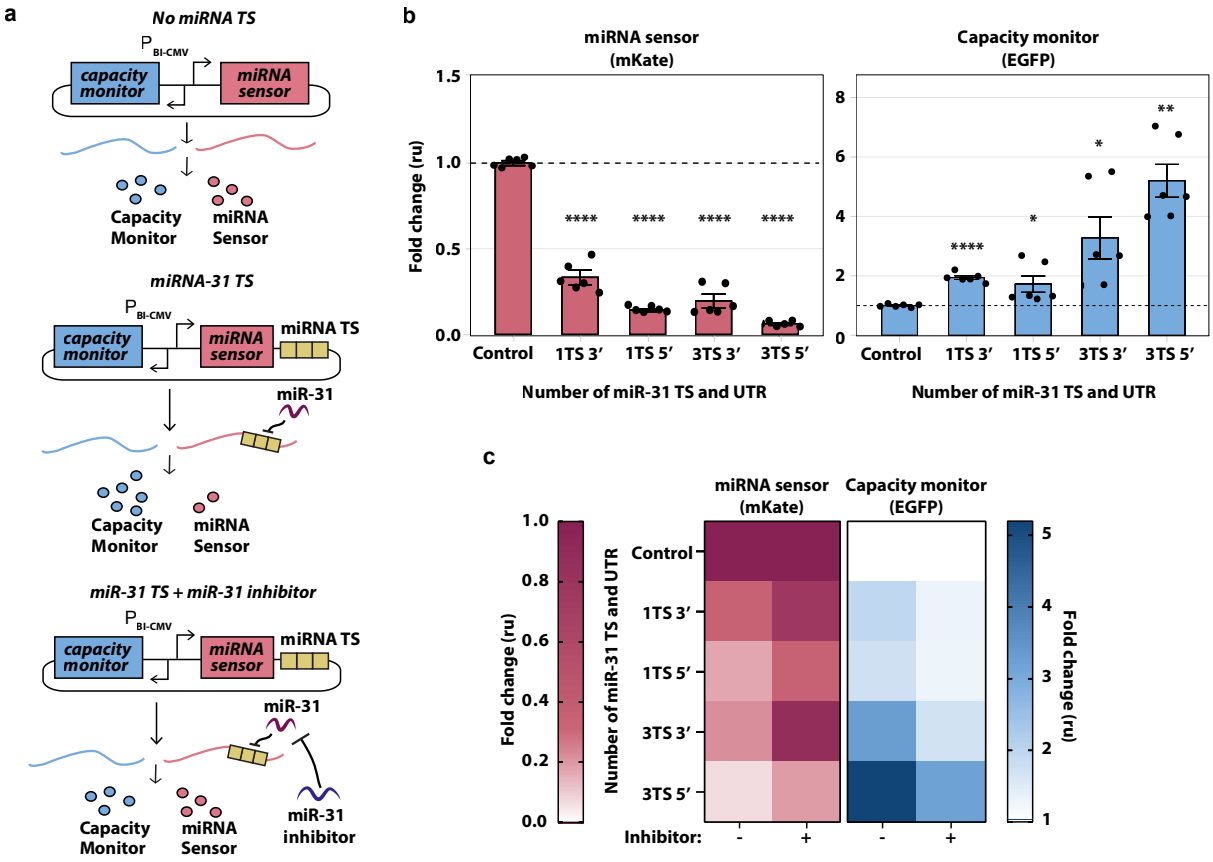

686 **Fig. 3. Impact of miRNA target sites number and location on burden. (a)** Schematics of experimental
687 design to infer miRNA-mediated cellular resources redistribution. EGFP (*capacity monitor*) and mKate
688 (*miRNA sensor*) are encoded on the same bi-directional CMV promoter plasmid. 1 or 3 TS for miR-31
689 (TS) are added either in the 3' or 5'UTR of mKate. Control: no miR31 TS. Hypothesis: in the absence
690 of miR-31 regulation, *capacity monitor* and *miRNA sensor* are expressed to a certain level (left). In
691 the presence of miR-31, lower *miRNA sensor* levels correlate with higher *capacity monitor* expression
692 (middle). This condition is reversed by a miR-31 inhibitor (right). **(b)** Fold change of *miRNA sensor* and
693 *capacity monitor* protein levels compared to control (set to 1). EGFP increases up to 5 fold with the
694 strongest downregulation of mKate (3TS 5'UTR). Flow cytometry data were acquired 48 hours
695 post-transfection and are plotted +/- SE. SE:standard error. ru: relative units. N=6 biological
696 replicates, unpaired T-test. p-value: ****<0.0001, ***<0.0005, **<0.005, *<0.05. **(c)** When miR31
697 activity was impaired by a miR-31 inhibitor, the rescue of mKate expression corresponds to reduced
698 EGFP levels, whereas both fluorescent proteins do not vary in the control. Flow cytometry data was
699 acquired 48 hours post-transfection and is plotted as a heatmap of the fold change. The fold change
700 is calculated as the ratio between the mean of 6 biological replicates and the corresponding mean in
701 the control condition. Corresponding bar plots and statistical analysis are reported in **Supplementary**
702 **Fig. 15**.

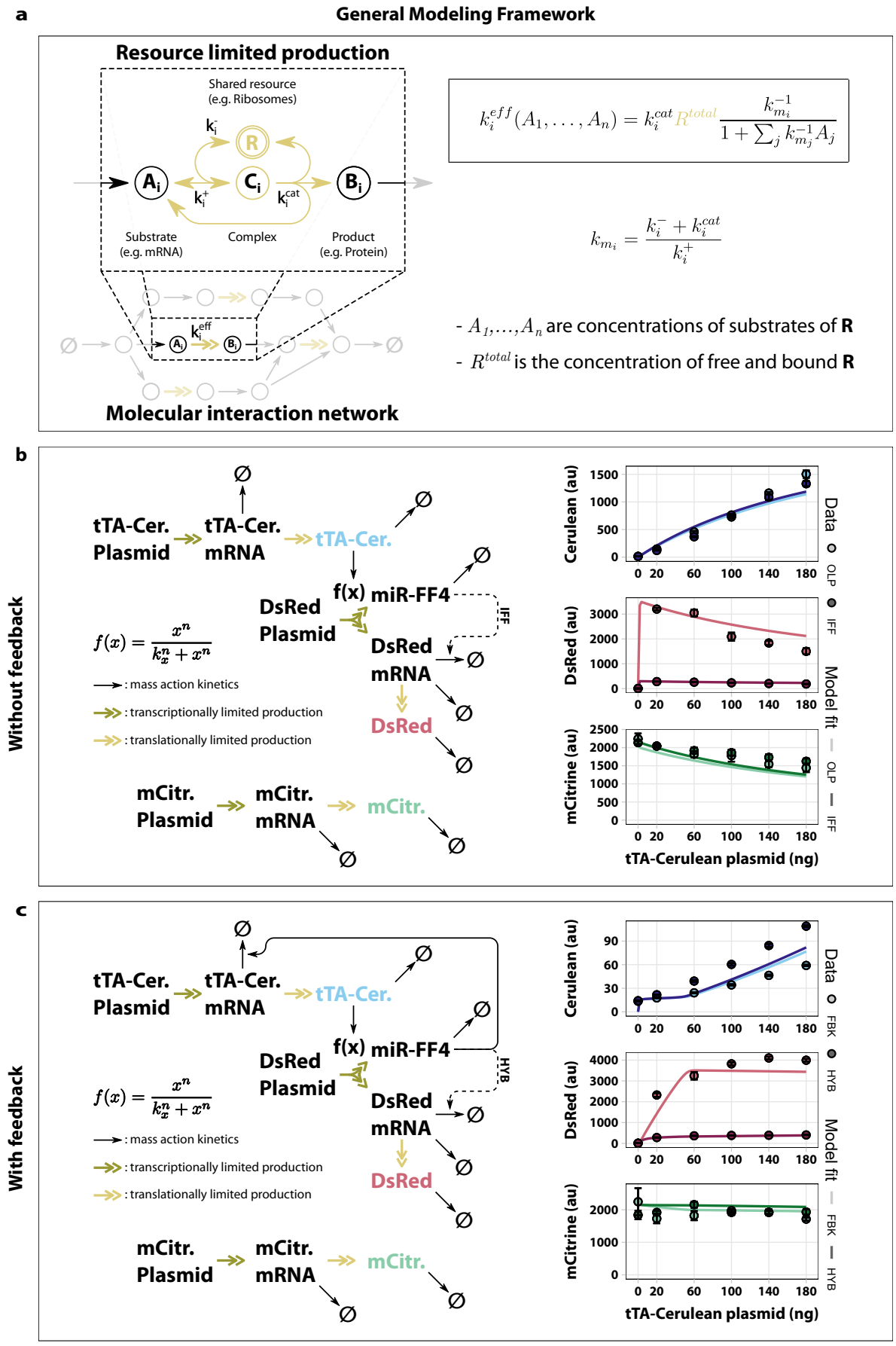
a
General Modeling Framework
Resource limited production
Shared resource
(e.g. Ribosomes)
R
Substrate
(e.g. mRNA)
Complex
Product
(e.g. Protein)
Molecular interaction network
- $A_1,\ldots,A_n$ are concentrations of substrates of R
- R^{total} is the concentration of free and bound R
b
Without feedback
tTA-Cer. Plasmid
tTA-Cer. mRNA
tTA-Cer.
f(x) miR-FF4
DsRed Plasmid
DsRed mRNA
DsRed
mCitr. Plasmid
mCitr. mRNA
mCitr.
: mass action kinetics
: transcriptionally limited production
: translationally limited production
Cerulean (au)
DsRed (au)
mCitrine (au)
tTA-Cerulean plasmid (ng)
Data
Model fit
OLP
IFF
c
With feedback
HYB
FBK

Fig. 4. A mathematical network model that factors in burden-induced coupling reproduces counter-intuitive experimental observations. (a) General framework for transforming molecular interaction network models. Existing models of molecular interaction networks can be transformed to include shared limiting resources by substituting k_i, the reaction rate of a resource limited production, with k^{eff}_i. Shown above an exemplary resource limited production are the detailed interactions between the substrate and the shared resource. The substrate A_i binds and unbinds the shared resource R with rates k^+_i and k^-_i, respectively. Binding of the substrate A_i to the shared resource R forms a complex C_i which releases the substrate A_i, the shared resource R and the product B_i with rate k^{cat}_i. Under quasi steady-state assumptions the equivalent reaction rate k^{eff}_i can be expressed as shown on the right. For simplification the parameters k^+_i, k^-_i and k^{cat}_i are lumped into k_{mi}. **(b) Limited shared translational resources reproduces non-monotonous dose-response in open-loop and incoherent feedforward circuit topologies.** On the left a graphical representation of a model for both the open-loop (OLP) and incoherent feedforward (IFF) topologies from Lillacci *et al.*[22] is shown. Transcriptional activation is modelled by a Hill-type function as shown. The solid arrows denote reactions assumed to follow the law of mass action. The model incorporates translational resources as introduced in panel A. These reactions are depicted as double headed arrows. The model was fit to data obtained by transiently transfecting HEK293T cells with increasing amounts of plasmid encoding tTA-Cerulean. The data and the fit are shown on the right. For a full description of the model see **Supplementary Note 3**. **(c) Limited shared translational resources reproduces non-monotonous dose-response in feedback and hybrid circuit topologies.** The model shown on the left is the same as in panel B with an additional negative feedback from miR-FF4 to tTA-mRNA. These topologies correspond to the feedback (FBK) and hybrid (HYB) topologies from Lillacci *et al.*[22] The activation of gene expression by tTA-Cerulean is modeled by a Hill-type function as shown in the center of the figure. Reactions with double headed arrows denote resource limited production reactions as introduced in panel A. Solid arrows are assumed to follow the law of mass action. The model was fit to experimental data obtained from transient transfections with increasing amounts of plasmid encoding tTA-Cerulean. A full description of the model equations can be found in Supplementary Note 3. A description of the models can be found in **Supplementary Note 3** and the parameter values obtained by fitting are summarized in **Supplementary Table 7**. Data were analysed 48 hours after transfection and is plotted +/- SE. SE: standard error. N=3 biological replicates.

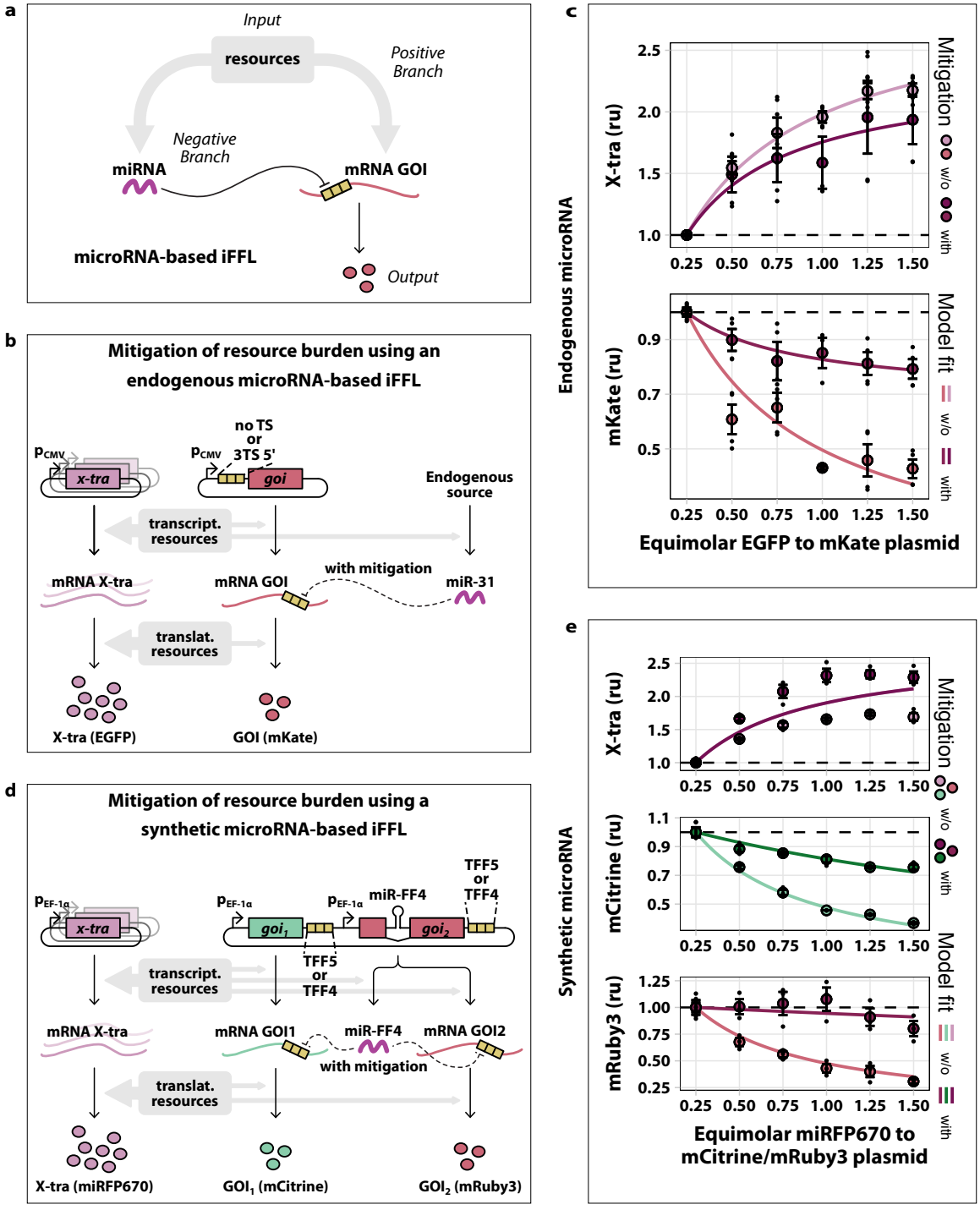

Fig. 5. Mitigating the effects of resource limitation with microRNA-based iFFL. (a) The microRNA-based incoherent feedforward loop (iFFL) motif. **(b)** Schematic representation of the mitigation system based on endogenous microRNA. At high copies number of the *X-tra*, resources are drawn away from the production of the *GOI* and miR-31. By sensing the resource availability and repressing the *GOI* less when there are fewer resources, the miRNA reduces the effect of limited resources. **(c)** Two plasmids were co-transfected into H1299 cells which respectively express the *X-tra*

739 gene (EGFP, panel b) and *GOI* (mKate, panel b) from strong constitutive CMV promoters. To limit the
740 amount of resources available to the expression of mKate, the copy number of the X-tra plasmid was
741 increased relative to the copy number of mKate. A mKate variant, which encodes three targets for
742 the microRNA miR-31 in it's 5' UTR, mitigates effects due to resource sharing when compared to a
743 variant lacking microRNA targets. The parameter values obtained by fitting are summarized in
744 **Supplementary Table 8**. N=3 biological replicates. **(d)** Schematic of the mitigation system based on
745 synthetic miRNA. In the presence of many copies of the *X-tra* gene, resources are drawn away from
746 the production of both of the *GOIs* and the miR-FF4. Due to lower production of miR-FF4 the *GOIs*
747 are less repressed. This compensates for the reduced availability of resources. **(e)** A plasmid encoding
748 both the fluorescent protein mCitrine (*GOI*, panel d) and an intronically expressed microRNA
749 (miR-FF4, panel d) under the control of strong constitutive promoters was co-transfected into
750 HEK293T cells with increasing amounts of a plasmid expressing the *X-tra* gene (miRFP670, panel d)
751 also under the control of a strong constitutive promoter. The impact of resource limitation on both
752 *GOIs* was reduced when they contained three miR-FF4 targets in their 3' UTRs compared to when
753 they contained three mismatched miR-FF5 targets. The parameter values obtained by fitting are
754 summarized in **Supplementary Table 9**. N=3 biological replicates. A description of the models can be
755 found in **Supplementary Note 4**. Flow cytometry data were acquired 48h post-transfection and are
756 plotted +/- SE. SE:standard error. ru: relative units.

References

1. Carrión, A. M., Link, W. A., Ledo, F., Mellström, B. & Naranjo, J. R. DREAM is a Ca2+-regulated transcriptional repressor. *Nature* **398**, 80–84 (1999).
2. Bamforth, S. D. *et al.* Cardiac malformations, adrenal agenesis, neural crest defects and exencephaly in mice lacking Cited2, a new Tfap2 co-activator. *Nat. Genet.* **29**, 469–474 (2001).
3. Liu, W. *et al.* Mutations in AXIN2 cause colorectal cancer with defective mismatch repair by activating β-catenin/TCF signalling. *Nature Genetics* **26**, 146–147 (2000).
4. Stuible, M. *et al.* Optimization of a high-cell-density polyethylenimine transfection method for rapid protein production in CHO-EBNA1 cells. *J. Biotechnol.* **281**, 39–47 (2018).
5. Xie, M. *et al.* β-cell-mimetic designer cells provide closed-loop glycemic control. *Science* **354**, 1296–1301 (2016).
6. Siciliano, V. *et al.* Engineering modular intracellular protein sensor-actuator devices. *Nat. Commun.* **9**, 1881 (2018).
7. Caliendo, F., Dukhinova, M. & Siciliano, V. Engineered Cell-Based Therapeutics: Synthetic Biology Meets Immunology. *Front Bioeng Biotechnol* **7**, 43 (2019).
8. MacDonald, J. T. & Siciliano, V. Computational Sequence Design with R2oDNA Designer. *Methods Mol. Biol.* **1651**, 249–262 (2017).
9. di Bernardo, D., Marucci, L., Menolascina, F. & Siciliano, V. Predicting synthetic gene networks. *Methods Mol. Biol.* **813**, 57–81 (2012).
10. Xiang, Y., Dalchau, N. & Wang, B. Scaling up genetic circuit design for cellular computing: advances and prospects. *Nat. Comput.* **17**, 833–853 (2018).
11. Borkowski, O., Ceroni, F., Stan, G.-B. & Ellis, T. Overloaded and stressed: whole-cell considerations for bacterial synthetic biology. *Curr. Opin. Microbiol.* **33**, 123–130 (2016).
12. Ceroni, F., Algar, R., Stan, G.-B. & Ellis, T. Quantifying cellular capacity identifies gene expression designs with reduced burden. *Nat. Methods* **12**, 415–418 (2015).
13. Li, G.-W., Burkhardt, D., Gross, C. & Weissman, J. S. Quantifying absolute protein synthesis rates reveals principles underlying allocation of cellular resources. *Cell* **157**, 624–635 (2014).
14. Scott, M., Gunderson, C. W., Mateescu, E. M., Zhang, Z. & Hwa, T. Interdependence of cell growth and gene expression: origins and consequences. *Science* **330**, 1099–1102 (2010).
15. Carbonell-Ballestero, M., Garcia-Ramallo, E., Montañez, R., Rodriguez-Caso, C. & Macía, J. Dealing with the genetic load in bacterial synthetic biology circuits: convergences with the Ohm's law. *Nucleic Acids Res.* **44**, 496–507 (2016).
16. Qian, Y., Huang, H.-H., Jiménez, J. I. & Del Vecchio, D. Resource Competition Shapes the Response of Genetic Circuits. *ACS Synth. Biol.* **6**, 1263–1272 (2017).
17. Weiße, A. Y., Oyarzún, D. A., Danos, V. & Swain, P. S. Mechanistic links between cellular

792 trade-offs, gene expression, and growth. *Proc. Natl. Acad. Sci. U. S. A.* **112**, E1038–47 (2015).
793 18. Gyorgy, A. *et al.* Isocost Lines Describe the Cellular Economy of Genetic Circuits. *Biophys. J.* **109**,
794 639–646 (2015).
795 19. Huang, H.-H., Qian, Y. & Del Vecchio, D. A quasi-integral controller for adaptation of genetic
796 modules to variable ribosome demand. *Nat. Commun.* **9**, 5415 (2018).
797 20. Ceroni, F. *et al.* Burden-driven feedback control of gene expression. *Nat. Methods* **15**, 387–393
798 (2018).
799 21. Kafri, M., Metzl-Raz, E., Jona, G. & Barkai, N. The Cost of Protein Production. *Cell Rep.* **14**, 22–31
800 (2016).
801 22. Lillacci, G., Benenson, Y. & Khammash, M. Synthetic control systems for high performance gene
802 expression in mammalian cells. *Nucleic Acids Res.* **46**, 9855–9863 (2018).
803 23. Siciliano, V. *et al.* MiRNAs confer phenotypic robustness to gene networks by suppressing
804 biological noise. *Nat. Commun.* **4**, 2364 (2013).
805 24. Carignano, A., Mukherjee, S., Singh, A. & Seelig, G. Extrinsic Noise Suppression in Micro RNA
806 mediated Incoherent Feedforward Loops. *bioRxiv* 422394 (2018) doi:10.1101/422394.
807 25. Strovas, T. J., Rosenberg, A. B., Kuypers, B. E., Muscat, R. A. & Seelig, G. MicroRNA-based
808 single-gene circuits buffer protein synthesis rates against perturbations. *ACS Synth. Biol.* **3**,
809 324–331 (2014).
810 26. Qin, J. Y. *et al.* Systematic comparison of constitutive promoters and the doxycycline-inducible
811 promoter. *PLoS One* **5**, e10611 (2010).
812 27. Lu, J., Zhang, F. & Kay, M. A. A Mini-intronic Plasmid (MIP): A Novel Robust Transgene Expression
813 Vector In Vivo and In Vitro. *Mol. Ther.* **21**, 954–963 (2013).
814 28. Kallehauge, T. B. *et al.* Ribosome profiling-guided depletion of an mRNA increases cell growth
815 rate and protein secretion. *Sci. Rep.* **7**, 40388 (2017).
816 29. Wroblewska, L. *et al.* Mammalian synthetic circuits with RNA binding proteins for RNA-only
817 delivery. *Nat. Biotechnol.* **33**, 839–841 (2015).
818 30. Cella, F., Wroblewska, L., Weiss, R. & Siciliano, V. Engineering protein-protein devices for
819 multilayered regulation of mRNA translation using orthogonal proteases in mammalian cells.
820 *Nat. Comm.* **9**, 4392 (2018).
821 31. Gam, J. J., Babb, J. & Weiss, R. A mixed antagonistic/synergistic miRNA repression model enables
822 accurate predictions of multi-input miRNA sensor activity. *Nat. Commun.* **9**, 2430 (2018).
823 32. Ameres, S. L. & Zamore, P. D. Diversifying microRNA sequence and function. *Nat. Rev. Mol. Cell*
824 *Biol.* **14**, 475–488 (2013).
825 33. Meleady, P. *et al.* Sustained productivity in recombinant Chinese hamster ovary (CHO) cell lines:
826 proteome analysis of the molecular basis for a process-related phenotype. *BMC Biotechnol.* **11**,

827 78 (2011).
828 34. Alles, J. *et al.* An estimate of the total number of true human miRNAs. *Nucleic Acids Res.* **47**,
829 3353–3364 (2019).
830 35. Thomson, D. W., Bracken, C. P. & Goodall, G. J. Experimental strategies for microRNA target
831 identification. *Nucleic Acids Res.* **39**, 6845–6853 (2011).
832 36. Robertson, B. *et al.* Specificity and functionality of microRNA inhibitors. *Silence* **1**, 10 (2010).
833 37. Chou, T. C. & Talaly, P. A simple generalized equation for the analysis of multiple inhibitions of
834 Michaelis-Menten kinetic systems. *J. Biol. Chem.* **252**, 6438–6442 (1977).
835 38. Rondelez, Y. Competition for catalytic resources alters biological network dynamics. *Phys. Rev.*
836 *Lett.* **108**, 018102 (2012).
837 39. Bleris, L. *et al.* Synthetic incoherent feedforward circuits show adaptation to the amount of their
838 genetic template. *Mol. Syst. Biol.* **7**, 519 (2011).
839 40. Zechner, C., Seelig, G., Rullan, M. & Khammash, M. Molecular circuits for dynamic noise filtering.
840 *Proc. Natl. Acad. Sci. U. S. A.* **113**, 4729–4734 (2016).
841 41. Tian, W. *et al.* High-throughput functional microRNAs profiling by recombinant AAV-based
842 microRNA sensor arrays. *PLoS One* **7**, e29551 (2012).
843 42. Gambardella, G. *et al.* The impact of microRNAs on transcriptional heterogeneity and gene
844 co-expression across single embryonic stem cells. *Nat. Commun.* **8**, 14126 (2017).
845 43. Cookson, N. A. *et al.* Queueing up for enzymatic processing: correlated signaling through
846 coupled degradation. *Mol. Syst. Biol.* **7**, 561 (2011).
847 44. Segall-Shapiro, T. H., Sontag, E. D. & Voigt, C. A. Engineered promoters enable constant gene
848 expression at any copy number in bacteria. *Nat. Biotechnol.* **36**, 352–358 (2018).
849 45. Jones, R. D. *et al.* An endoribonuclease-based feedforward controller for decoupling
850 resource-limited genetic modules in mammalian cells. *Synthetic Biology* 856 (2019).
851 46. Chassin, H. *et al.* A modular degron library for synthetic circuits in mammalian cells. *Nat.*
852 *Commun.* **10**, 2013 (2019).
853 47. Charlesworth, C. T. *et al.* Identification of preexisting adaptive immunity to Cas9 proteins in
854 humans. *Nat. Med.* **25**, 249–254 (2019).
855 48. You, L. *et al.* Advancements and Obstacles of CRISPR-Cas9 Technology in Translational Research.
856 *Mol Ther Methods Clin Dev* **13**, 359–370 (2019).
857 49. Ando, H., Hirose, M., Kurosawa, G., Impey, S. & Mikoshiba, K. Time-lapse imaging of microRNA
858 activity reveals the kinetics of microRNA activation in single living cells. *Sci. Rep.* **7**, 12642 (2017).
859 50. Xie, Z., Wroblewska, L., Prochazka, L., Weiss, R. & Benenson, Y. Multi-input RNAi-based logic
860 circuit for identification of specific cancer cells. *Science* **333**, 1307–1311 (2011).
861 51. Matsuura, S. *et al.* Synthetic RNA-based logic computation in mammalian cells. *Nat. Comm.* **9**,

862 4847 (2018).
863 52. Miki, K. *et al.* Efficient Detection and Purification of Cell Populations Using Synthetic MicroRNA
864 Switches. *Cell Stem Cell* **16**, 699–711 (2015).
865 53. Grieger, J. C. & Samulski, R. J. Packaging capacity of adeno-associated virus serotypes: impact of
866 larger genomes on infectivity and postentry steps. *J. Virol.* **79**, 9933–9944 (2005).
867 54. Geisler, A. & Fechner, H. MicroRNA-regulated viral vectors for gene therapy. *World J Exp Med* **6**,
868 37–54 (2016).
869 55. Seyhan, A. A. A multiplexed miRNA and transgene expression platform for simultaneous
870 repression and expression of protein coding sequences. *Mol. Biosyst.* **12**, 295–312 (2016).
871 56. Laganà, A. *et al.* miR-Synth: a computational resource for the design of multi-site multi-target
872 synthetic miRNAs. *Nucleic Acids Res.* **42**, 5416–5425 (2014).
873 57. Yuan, Y. *et al.* Model-guided quantitative analysis of microRNA-mediated regulation on
874 competing endogenous RNAs using a synthetic gene circuit. *PNAS* **112**, 3158–3163 (2015).
875 58. Ying, Q.-L. *et al.* The ground state of embryonic stem cell self-renewal. *Nature* **453**, 519–523
876 (2008).
877 59. Lee, M. E., DeLoache, W. C., Cervantes, B. & Dueber, J. E. A Highly Characterized Yeast Toolkit for
878 Modular, Multipart Assembly. *ACS Synth. Biol.* **4**, 975–986 (2015).